Device-scale CFD Modeling of Gas-liquid Multiphase Flow and Amine Absorption for CO_2 Capture

Wenxiao Pan[1*], Janine Galvin[2], Wei Ling Huang[1], Zhijie Xu[3], Xin Sun[4], Zhen Fan[5], and Kunlei Liu[5]

[1]Department of Mechanical Engineering, University of Wisconsin-Madison, Madison, WI 53706

[*]Email: wpan9@wisc.edu

[2]National Energy Technology Laboratory, Albany, OR 97321

[3]Advanced Computing, Mathematics & Data Division, Pacific Northwest National Laboratory, WA 99352

[4]Energy and Transportation Science Division, Oak Ridge National Laboratory, TN 37830

[5]Center for Applied Energy Research, University of Kentucky, Lexington, KY 40511

Abstract

In this work, we aim to develop a validated device-scale CFD model that can quantitatively capture both hydrodynamics and CO_2 capture efficiency for an amine-based solvent absorber column with a random Pall ring packing. Eulerian porous-media approach and two-fluid model were employed, in which the momentum and mass transfer equations were closed by literature-based empirical closure models. We proposed a hierarchical approach for calibrating the parameters in the closure models to make them accurate for the studied packed column. Specifically, a parameter in the closure for momentum transfer was first calibrated based on a single experimental data. With this calibrated parameter, a parameter in the closure for mass transfer was next calibrated at a single operating condition. Last, the closure of wetting area was calibrated for each gas velocity at three different liquid flow rates. For each calibration, cross validations were pursued using the experimental data under operating conditions different from those used for calibrations. This

hierarchical approach can be generally applied to develop validated device-scale CFD models for different absorption columns.

Keywords: CO_2 capture; Amine absorber; Packed Column; Computational fluid dynamics; Validation

1. Introduction

One method of removing CO_2 from a flue gas stream is through liquid solvent absorption. The absorption can be classified as physical or chemical absorption with chemical solvents preferred due to higher solubility and absorption rate. Solvent absorption is usually carried out in a countercurrent column where the gas ascends, and the liquid descends. The purpose is to preferentially dissolve CO_2 into the liquid solvent. The absorber column is typically filled with engineering packings that provide the desirable surface area for gas-liquid contact. Large surface area is important for solvent-based capture because very little reaction will occur without adequate mixing of the gas and liquid. For example, if gas is simply bubbled through a tank of liquid, some degree of mixing will occur. But since reaction only occurs where the gas and liquid have direct contact, such mixing will result in a very low capture efficiency per solvent volume.

The flow dynamics of the liquid film is important in solvent absorption because efficiency of CO_2 absorption is closely related to the topographical structure and distribution of the liquid film within the packing [1]. Numerous experimental studies have been conducted to investigate the pressure drop, liquid holdup, and mass transfer in an amine absorber with structured-packings [2-4]. Although experimental studies have made continuous progress, they are still expensive and time consuming. To accelerate advancement and commercialization of CO_2 capture technologies, computational fluid dynamics (CFD) modeling provides an efficient and cost-effective tool offering high fidelity and quantitative insights into the absorption processes, consequently enabling trouble shooting and optimization of design and operating conditions of the packed column. However, one of the main challenges in developing a CFD model for solvent absorption is its multi-scale nature. The column size is characterized by length scales of $\mathcal{O}(1)$ m (in

diameter) to $\mathcal{O}(10)$ m (in height), while the characteristic dimension of the packing is much smaller. For example, structured packings, such as Raschig or Pall Rings, typically have dimensions ranging from 16-80 mm [5]. The length scale of a typical layer of corrugated structured packing is on the order of 20 centimeters [6]. The corrugation height varies with the specific area of the packing from a few millimeters to several centimeters [7]. Finally, the dimension of liquid film thickness is on the order of tenths of millimeters for structured packing [6]. These scales cannot be resolved simultaneously within a single computational model. For example, the volume of fluid (VOF) model is an appropriate numerical method for simulating two phase flows where the interface between the gas-liquid phases is important. However, it requires the geometry of each packing element be faithfully modeled. It is computationally infeasible to run computations at large scales while considering the gas-liquid interaction in the fully resolved geometry of the packing. Thus, simulations based on VOF are confined to small scales relevant to the film thickness.

In most existing device-scale CFD studies concerning absorption columns, an Eulerian-based continuum formulation was typically used, in which the structured-packing was represented by a porous media. Owens el al. [8] developed a gas-phase Eulerian model to calculate the dry gas pressure drop in the real three-dimensional (3D) packing column. Tung and Dhir [9] developed a 1D two-phase model with drag forces between phases to investigate the hydrodynamics in a packing column. Asendrych et al. applied such a two-phase approach along with mass transfer to model CO_2 absorption [10], in which a series of parametric simulations showed that CO_2 capture efficiency was mostly influenced by the ratio of liquid (aqueous amine solution) to gas (flue gases) mass fluxes. The simulation results were compared to the available literature and experimental data, and an overprediction of CFD model on the CO_2 capture efficiency was found, especially for low and intermediate liquid to gas ratios [10]. Further, Fourati et al. [11] included capillary pressure and liquid dispersion forces into a two-phase porous-media model based on the work of Iliuta et al [12], who developed a slit model for liquid film flow applied to structured packing. The porous resistance terms (i.e., gas-solids and liquid-solids) are essentially permeabilities with an Ergun form having both viscous and inertial effects. The gas-liquid interfacial term is of comparable form except for the definition of the relative

velocity. Pham et al. [13] used a similar modeling strategy but also considered mass transfer to model CO_2 capture from natural gas using a 3D geometry. Their model considered porous resistance, a gas−liquid interfacial drag force, and a liquid dispersion force. Kim et al. [14] applied this same model to investigate the hydrodynamics and CO_2 removal efficiency of a pilot-scale amine absorber with the structured-packing. The Ergun coefficients were calibrated (two in the porous resistance models and two in the gas-liquid interaction term) using the experimental data to capture the hydrodynamic characteristics of the specific structured-packing of interest. The focus of this earlier effort [14] was on calibrating Ergun type coefficients for the interfacial drag and resistance terms based on liquid holdup and wet pressure drop data. Another investigation regarding a systematic approach for calibration of the interphase drag model for solvent absorption is explored by Finn et al [15]. In the present effort, we go beyond calibrating the hydrodynamics and examine the chemistry of the problem. That is, we calibrate our interfacial drag model but also parameters in the mass transfer model as discussed further below. We also accommodate variable physical properties as functions of temperature or concentration instead of constant properties as assumed in the earlier work [14].

The present work also focuses on the device-scale CFD modeling of CO_2 capture with amine-based solvent in an absorber column with randomly packed Pall rings. Similar to the previous studies, an Eulerian porous-media approach is employed. Namely, solvent absorption is numerically investigated using the Eulerian-Eulerian two fluid model in which the different phases are mathematically treated as interpenetrating continua. The volume fractions of each phase are assumed to be continuous functions of space and time. Interfacial drag terms are considered for momentum transfer between phases. Moreover, the mass transfer of CO_2 is modeled based on the two-film theory. Both the momentum and mass transfer equations are closed by empirical closure models.

The closure models adopted from the literature are based on physically motivated phenomenological considerations and/or on experimental measurements in systems wherein the microscale flow patterns are expected to differ from those in the present work. Specifically, these models were developed for flow in

packed beds and packing materials that may not resemble that in the randomly packed Pall ring absorber column studied herein. Hence, simply employing these models may not yield accurate predictions for either the hydrodynamics or CO_2 capture. As a result, the parameters in these semi-empirical closure models need to be calibrated using available experimental data. From this perspective, we have developed a hierarchical calibration approach so that the literature based empirical closure models are suitable for studying solvent absorption in the packed column and operating conditions specific to this study. Specifically, a parameter in the interfacial drag closure is first calibrated based on a single experimental data point on column level hydrodynamics. Then, with this calibrated parameter for hydrodynamics, a parameter in the two-film theory is also calibrated at a single operating condition to correctly reproduce the corresponding CO_2 capture efficiency. Finally, the model of wetting area is further calibrated for *each* gas velocity explored based on three experimental measurements of CO_2 capture efficiency at different liquid flow rates. The fully calibrated model is then used for predictions at other operating conditions as a cross validation effort. With this approach, a validated device-scale CFD model is developed that can quantitatively capture both hydrodynamics and CO_2 capture efficiency for an amine-based absorber column with a random Pall ring packing. Provided the appropriate experimental data, this method may be followed to calibrate a corresponding CFD model for a different absorption column.

The rest of this paper is organized as follows: Section 2 introduces the device-scale porous media CFD model with empirical formulations. Section 3.1 describes the geometry and material parameters. Section 3.2 presents the simulation results with comparison to the experimental data. We conclude in Section 4 with a discussion about the future work.

2. Porous media CFD model

Explicitly resolving the complex geometry of the packing structure at the device scale is computationally infeasible. Instead, the packing structure is approximated with an effective porous media formation [16]. With

this approach, depicting the intricacies of the packing boundaries and geometrical topology of the packing is avoided while the flow dynamics at the device scale can still be captured. For randomly packed beds, different levels of detail can be encompassed in a porous-media type approach, ranging from a mean porosity assigned to the whole bed, to an axially averaged radial porosity profile, to a statistical description of the geometry in terms of void fraction profiles [16]. In the present work, the packing region was regarded as a porous medium with a uniform mean porosity, where hydrodynamics of gas and liquid were modeled by porous resistance and drag force between the two phases. The conservation equations are hence derived based on the application of volume averaging to the microscopic description of the system.

2.1 Conservation Equations

Shown below are the continuity and momentum equations used in a reactive flow simulation for gas-liquid systems (e.g. [17-18]):

$$\frac{\partial}{\partial t}(\varepsilon_i \rho_i) + \nabla \cdot (\varepsilon_i \rho_i \mathbf{u}_i) = \sum_{n=1}^{N_i} R_{in}, \tag{1}$$

$$\frac{\partial}{\partial t}(\varepsilon_i \rho_i \mathbf{u}_i) + \nabla \cdot (\varepsilon_i \rho_i \mathbf{u}_i \mathbf{u}_\mathbf{i}) = -\varepsilon_i \nabla P_i + \nabla \cdot (\varepsilon_i \boldsymbol{\tau}_i) + \varepsilon_i \rho_i \mathbf{g} - F_{ij}\left(\mathbf{u}_i - \mathbf{u}_j\right) - F_{si}\mathbf{u}_i. \tag{2}$$

Here, ε_i represents the volume fraction of the ith phase, ρ_i is the density of the ith phase, and $\mathbf{u}_\mathbf{i}$ is the cell velocity of the ith phase. In Eq. (1), N_i is the number of chemical species comprising the ith phase and R_{in} represents the rate of formation of the nth species in the ith phase. The term on the right-hand side represents the formation or consumption of mass attributed to interphase mass transfer from chemical reactions or physical processes. In the momentum balance (Eq. (2)), P_i is the ith phase pressure, $\boldsymbol{\tau}_i$ is the shear stress, $\mathbf{g}$ is gravitational acceleration, and F_{ij} and F_{si} are the interphase momentum exchange terms. The respective terms on the right-hand side represent the pressure gradient, stress, gravitation force, interphase momentum exchange due to interfacial forces.

The conservation of species mass equation for the nth species in the ith phase is

$$\frac{\partial}{\partial t}(\varepsilon_i \rho_i X_{in}) + \nabla \cdot (\varepsilon_i \rho_i \mathbf{u}_i X_{in}) = \nabla \cdot \left(\mathcal{D}_{gn} \nabla X_{in}\right) + R_{in} \tag{3}$$

where X_{in} and $\mathcal{D}_{in}$ are the nth species mass fraction and diffusion coefficient of the nth species in the ith phase, respectively. The specific chemistry scheme and corresponding reaction models implemented are used to describe the rate of production/consumption of each chemical species present in the system (R_{in}). The summation of this term over all species present in the given phase becomes a source term in the respective phase continuity equation (see Eq. (1)).

The conservation of internal energy is presented here in terms of temperature:

$$\varepsilon_i \rho_i C_{pi} \left[\frac{\partial T_i}{\partial t} + \mathbf{u}_i \cdot \nabla T_i\right] = -\nabla \cdot (-\lambda_i \nabla T_i) - \sum_{n=1}^{N_i} h_{in} R_{in} + S_i \tag{4}$$

where, C_{pi} is the ith phase mixture specific heat, T_i is the ith phase temperature, and λ_i is the ith phase thermal conductivity. The first two terms on the right-hand side include the conductive heat flux described by Fourier's Law and changes in internal energy accompanying species formation or destruction due to chemical reactions and phase changes. The last term, S_i, is a general source term which includes interphase heat transfer (convective transfer) and enthalpy transfer accompanying interphase mass transfer (see [19]). Radiant heat transfer has been neglected.

Coupling between the phases is achieved through the interphase heat, mass and momentum exchange terms. To solve the above governing equations, the unknown terms require constitutive relations for closure.

2.2 Hydrodynamic Model Closures

To properly model the hydrodynamics of counter-current gas liquid two phase flow through a packed column, the physics relating to the local film flow operation must be incorporated into the multiphase flow model framework. However, appropriate closure models for this system that capture the micro/meso-scale behavior of the liquid film on a packing material are lacking. The most suitable models currently available in the literature are largely based on co-current trickle bed reactor work. Considerable efforts have been

made in the study of the hydrodynamics of trickle bed reactors. Accordingly, several constitutive relations have been proposed to describe the phase interactions from empirical approaches to those with a more fundamental physical basis. Several well-known methods include a relative permeability type model [20], the slit model [21-22], and the two fluid interaction model [23]. In this effort, the interphase interaction model of Attou et al. [23] was employed. This model is derived assuming gas-liquid flow through a fixed bed of solid particles. The packing surface is completely covered by the liquid film and the gas flows in the central zone so that the gas and liquid phases are completely separated by a smooth interface. With this depiction, the form of the interaction forces as they relate to the local microscopic forces is derived from the momentum balance equations. The forces are then closed by considering the Kozeny-Carman equation, or more aptly the Ergun relation that accounts for both viscous and inertia contributions, applied to each fluid and considering the two-phase pattern (for details see [23]). Note that pressure drop in a packed bed, and so formulations of the interphase coupling terms, are often correlated with Ergun's relation or a variation thereof.

For ease of implementation, the interphase coupling terms proposed by Attou et al [23] are rewritten here in terms of interstitial velocities and phase volumes (instead of superficial velocities and saturation) [24]. Here, the tortuosity factor (inversion of liquid saturation) was omitted from the liquid-solid interaction term:

$$F_{gl} = \varepsilon_g \left(\frac{C_1 \mu_g (1-\varepsilon_g)^2}{\varepsilon_g^2 d_p^2} \left[\frac{\varepsilon_s}{1-\varepsilon_g} \right]^{\frac{2}{3}} + \frac{C_2 \rho_g (1-\varepsilon_g) |\mathbf{u}_g - \mathbf{u}_l|}{\varepsilon_g d_p} \left[\frac{\varepsilon_s}{1-\varepsilon_g} \right]^{\frac{1}{3}} \right) \tag{5}$$

$$F_{sg} = \varepsilon_g \left(\frac{C_1 \mu_g (1-\epsilon_g)^2}{\varepsilon_g^2 d_p^2} \left[\frac{\varepsilon_s}{1-\varepsilon_g} \right]^{\frac{2}{3}} + \frac{C_2 \rho_g (1-\varepsilon_g) |\mathbf{u}_g|}{\varepsilon_g d_p} \left[\frac{\varepsilon_s}{1-\varepsilon_g} \right]^{\frac{1}{3}} \right) \tag{6}$$

$$F_{sl} = \varepsilon_l \left(\frac{C_1 \mu_l \varepsilon_s^2}{\varepsilon_l^2 d_p^2} + \frac{C_2 \rho_l \varepsilon_s |\mathbf{u}_l|}{\varepsilon_l d_p} \right) \tag{7}$$

where μ_i is the viscosity of the ith phase, C_1 and C_2 are constants, and other quantities are as before. The subscripts $i = g, l$ and s refer to the gas, liquid and solids (packing) phase respectively. In this work, the

values of C_1 and C_2 are taken as 180 and 1.8, respectively. The quantity d_p is referred to as the surface-volume equivalent sphere diameter of the particles ($d_p \equiv 6V_p/S_p$ where V_p and S_p are the volume and area of the particle respectively). As noted by Kuzeljevic and Dudukovic [25] the phase interaction closures will reduce the speed at which the liquid front travels and increase the liquid saturation of the front.

When two immiscible fluids are in contact with each other, interfacial surface tension may cause the fluids to have different pressures. This discontinuity in pressure is referred to as capillary pressure. In this effort, a capillary pressure model was introduced [1] but not employed by any of the simulations from which results are presented . Thus, in those cases the liquid and gas phase experience the same pressure. This may be a reasonable approximation when gravity and inertia are important and capillary forces are negligible [16, 26]. A few test cases also revealed the results to be insensitive to the presence of a capillary pressure term (not shown).

The shear stress term in the fluid phases is described using a Newtonian form requiring a value for effective viscosity (μ_i), which can have contributions from molecular viscosity and turbulent viscosity. In the latter case, a turbulence model must be included for porous media, yielding additional closure equations. Such a model is not considered here because turbulent viscosity at low gas velocity can be ignored. Hence, μ_i is simply the molecular viscosity of the fluid.

2.3 Mass Transfer Model Closures

To develop a comprehensive model for solvent absorption requires description of the underlying mechanism by which the absorption takes place. That is, the model must encompass mass transfer of CO_2 from the bulk gas to the solvent, solution reactions between CO_2 and solvent species, and the associated kinetic regimes.

2.3.1 Solvent Absorption Model

Monoethanolamine (MEA) is a common chemical solvent for CO_2 absorption and the focus of this study. The reaction between CO_2 and primary and secondary amines is often represented by a two-step mechanism

[27]. The mechanism first proceeds through reaction of MEA (RNH_2) with CO_2 to form a zwitterion intermediate ($RNH_2^+COO^-$ with R=–C_2H_2OH). The zwitterion is subsequently deprotonated by some base to form a carbamate ($RNHCOO^-$). Any base (RNH_2, OH^-, H_2O, HCO_3^- and CO_3^-) may contribute to the deprotonation of the zwitterion. When formation of the carbamate is almost instantaneous compared to reversion of the zwitterion, the overall conversion of CO_2 may be written as the following irreversible reaction [28-29]:

$$CO_2 + 2RNH_2 \longrightarrow RNH_3^+ + RNHCOO^- \tag{8}$$

For CO_2/MEA mole ratio less than 0.5, the rate of bicarbonate formation is considered insignificant [30], and hence this reaction scheme neglects bicarbonate formation.

For CO_2–MEA system where carbamate formation is considered the main reaction the reaction rate is considered first order with respect to CO_2 and MEA in terms of molar concentrations and second order overall:

$$r = k_2 C_{CO_2} C_{RNH_2} \tag{9}$$

The reaction rate constant (k_2) is characterized by a rate expression given by Hikita [31]

$$\log(k_2) = 10.99 - \frac{2152}{T_l} \tag{10}$$

with unit $\frac{liter}{g\ mol{\cdot}s}$ and T_l is the absolute temperature in $Kelvin$.

It is only when CO_2 enters the liquid phase that it can react with the MEA solution. Therefore, the overall rate for absorption of CO_2 in an aqueous solution of MEA must account for both mass transfer and chemical reaction rate. Here, the interphase mass transfer step is considered independent from the subsequent chemical reaction(s):

1) CO_2 transfer from the gas to liquid phase:

$$CO_2(g) \rightarrow CO_2(l), \tag{11}$$

2) Carbamate formation described by Eq. (8) (the primary homogenous liquid phase reaction as described in the previous section).

For the first step, the mass transfer from the gas bulk into the gas boundary layer, across the interface and from the interface through the liquid reaction boundary layer and finally into the liquid bulk need to be established. Recall that the Eulerian-Eulerian approach does not perform interface tracking and so is unable to capture the wetting characteristics at the gas-liquid interface. Thus, this information must be introduced through an appropriate model correlation. There are many different levels of models and correlations to describe this process in the literature. In this effort, film theory is used (see [32]).

In the two-film model, it is assumed that resistance to mass transfer occurs in a thin film adjacent to the phase interphase. Mass transfer in this interface occurs by steady state molecular diffusion. Outside the film in the fluid bulk mixing is sufficiently high so that only diffusion transport normal to the interface occurs. For CO_2 in MEA it is assumed that the reaction is fast enough that the reaction takes place only in the liquid film [33]. Accordingly, the bulk of the liquid is in equilibrium.

Following the work of Pandya [33], the mass flux of absorbed component N_i across the gas-liquid interface at steady state can be presented in terms of a mass transfer coefficient and driving force. The general form of the flux equations is:

$$N_{CO_2} = k_g a\left(p_{CO_2} - p_{CO_2}^{\text{interface}}\right) \tag{12}$$

$$N_{CO_2} = k_l^{\circ} a\mathrm{E}\left(C_{CO_2}^{\text{interface}} - C_{CO_2}\right) \tag{13}$$

where k_g and k_l^o are the physical mass transfer coefficients of the CO_2 species in the gas and liquid phase, respectively, a is the interfacial surface area per unit volume of bed, C_{CO_2} and $C_{CO_2}^{interface}$ is the molar concentration of CO_2 in the bulk and interface, p_{CO_2} and $p_{CO_2}^{\text{interface}}$ is the partial pressure of CO_2 in the bulk and interface, and E is the enhancement factor.

Through a combination of the two flux equations (Eqs. (12) and (13)) and using Henry's law for vapor liquid equilibrium, an expression for the interfacial concentration of CO_2 is obtained as follows

$$p_{CO_2}^{\text{interface}} = \frac{p_{CO_2} + \frac{k_l^{\circ} E}{k_g} C_{CO_2}}{1 + \frac{k_l^{\circ} E}{k_g H}} \tag{14}$$

where H is Henry's solubility constant $\left(C_{CO_2}^{\text{interface}} = \frac{p_{CO_2}^{\text{interface}}}{H}\right)$. Using this expression for the partial pressure at the interface, the flux of CO_2 from the gas to liquid phase is described. To evaluate this expression requires knowledge of the physical-chemical properties of the fluids involved in the process including gas and liquid phase mass transfer coefficients, interfacial area, and solubility. The first two are discussed in more detail below. Following the work of Hiwale [34] the N_2O analogy is used to estimate the solubility of CO_2 in MEA (H) with correlations for both the solubility of N_2O and CO_2 in water [35] and the solubility of N_2O in pure MEA [36].

The acceleration of mass transfer due to chemical reaction in the interfacial region is typically accounted for by what is known as the enhancement factor. The functional dependency of the enhancement factor is determined by the specific kinetic reaction taking place in the liquid film. However, the contribution of the enhancement factor is presently omitted, i.e., $\mathrm{E} = 1$. In the current implementation, the overall chemistry model would become inconsistent for E other than unity as in that case the rate of CO_2 transfer already encompasses the effects of subsequent chemical reaction of CO_2, which is also described separately. To accommodate the concept of an enhancement factor would require a more detailed model describing the evolution of CO_2 concentration in the liquid phase (i.e., liquid phase equilibrium model). Instead, the rate at which the carbamate formation occurs (Eq. (8)) is simply given by the kinetic expression (Eqs. (9) and (10)), while the rate of CO_2 mass transfer (Eq. (11)) is estimated by physical mass transfer model (Eqs. (12) and (14) with $\mathrm{E} = 1$).

2.3.2 Correlations for wetting area and mass transfer coefficients

To evaluate the absorption model above requires information on the physicochemical properties as well as on the mass-transfer coefficients and gas-liquid contact area. A number of empirical, and semi-theoretical models for predicting mass transfer in packed columns have been published in the literature (e.g., [36-37]). Complicating physics (interfacial behavior, complex geometry/structure effects) related to this system are accommodated into the model framework through these terms. The correlations will depend on packing type and system conditions, and therefore, are not universally applicable. That is, these correlations will have limitations restricting their suitability for a specific application.

In the present work, an empirical correlation by Onda [38] is adopted as the baseline for predicting the gas-liquid contact area and gas and liquid-side mass transfer coefficients:

$$\frac{a_w}{a_t} = 1 - \exp\left(-1.45\frac{\sigma_c^{0.75} g^{0.05} L'^{0.4}}{\sigma^{0.95} a_t^{0.35} \mu_l^{0.1} \rho_l^{0.1}}\right) \tag{15}$$

$$k_l^o = 0.0051\left(\frac{L'}{a_w \mu_l}\right)^{\frac{2}{3}}\left(\frac{\mu_l}{\rho_l \mathcal{D}_{l,s}}\right)^{-\frac{1}{2}}\left(a_t D_p\right)^{0.4}\left(\frac{\mu_l g}{\rho_l}\right)^{\frac{1}{3}} \tag{16}$$

$$k_g = 5.23\left(\frac{G'}{a_t \mu_g}\right)^{0.7}\left(\frac{\mu_g}{\rho_g \mathcal{D}_{g,s}}\right)^{\frac{1}{3}}\left(a_t D_p\right)^{-2.0}\left(\frac{a_t \mathcal{D}_{g,s}}{RT}\right) \tag{17}$$

where a_w is the wetting surface area of packing per unit volume of bed; a_t is the total surface area of packing per unit volume of bed (also known as the specific area); R is the universal gas constant; T is the absolute temperature; D_p is the nominal size of the packing material (to distinguish it from d_p used in Eqs. (5)-(7)); σ_c is the critical surface tension of packing material; σ is the surface tension of liquid; L' is the superficial mass velocity of the liquid ($L' = |\boldsymbol{u}_l|\rho_l \varepsilon_l$); G' is the superficial mass velocity of the gas ($G' = |\boldsymbol{u}_g|\rho_g \varepsilon_g$); $\mathcal{D}_{g,s}$ is the diffusivity of the solute species in the gas phase; $\mathcal{D}_{l,s}$ is the diffusivity of the solute in the liquid phase. Here, solute refers to CO_2. The other symbols are as noted earlier.

Similar to Onda [38], the wetting surface of the packing is assumed here to be identical to the effective interfacial area (i.e., $a = a_w$). It is worth noting that these correlations were developed based on random

packed columns. That said, these correlations simply provide a mechanism to demonstrate this solvent absorption model, and as in the case of other closure quantities, may be replaced by a more suitable model depending upon the application of interest. The values of a_t, D_p, and σ_c will depend on the specific packing material and geometry features.

Evaluation of Eqs. (15) – (17) requires information on the density, viscosity and diffusivities of the representative gas and liquid. In these expressions, $\mathcal{D}_{g,s}$ is taken as the diffusivity of CO_2 in air, and is assigned a constant value $\left(\mathcal{D}_{g,s} = 0.16\frac{cm^2}{s}\right)$, and $\mathcal{D}_{l,s}$ is taken as the diffusivity of CO_2 in MEA solution $\left(\mathcal{D}_{l,s} = \mathcal{D}_{l,CO_2}\right)$. Here, the diffusivity of CO_2 in MEA solution is calculated from [39]: $\mathcal{D}_{l,CO_2} = 0.0235\, e^{-\frac{2119}{T}}\left(\frac{\mu_{MEA}}{\mu_{H_2O}}\right)^{0.8}$ in the unit of $\frac{cm^2}{s}$. The viscosity (μ_l) is taken as the viscosity of MEA (μ_{MEA}) based on the correlation provided by Weiland [40]. Similarly, the density of the liquid (ρ_l) is based on a partially loaded MEA solution described by Weiland. A value for surface tension is also required and the expression by Vazquez [41] for MEA and water is used. The density and viscosity of the gas are based on those of air as is described later in more detail.

2.4 Heat Transfer Model Closures

As noted earlier the main heat transfer mechanisms in the flow are interphase heat transfer (convective transfer) and enthalpy transfer accompanying interphase mass transfer. Default closures for the convective interphase heat transfer are employed [42-43], wherein the heat transfer coefficients are taken based on correlation of the Nusselt number. Default calculation for enthalpy transfer associated with mass transfer [19] is superseded by defining a single heat of reaction with a value taken from Gabrielsen [44]: -87.9 kJ/mol of CO_2. Specifically, the heat of reaction for CO_2 absorption into MEA is attributed to the CO_2 transfer step (Eq. (11)) and assigned to the liquid phase. The subsequent carbamate formation reaction (Eq. (8)) is assigned a heat of reaction of zero.

3. CFD Simulation

3.1 System Description

In this work, counter-current gas-liquid flow through a packing column is simulated using MFIX, an open source CFD software package. The geometry, physical properties and flow conditions are the same as those used in the experimental setup [2]: Specifically, the small scale absorber column is 0.1 m in inner diameter and 2 m in height with 1.75 m of effective packing, as depicted in Fig. 1. Three continuous phases are employed: a gas phase, a liquid phase, and a solid phase that represents a porous medium for the packing material. The packing is considered stationary (i.e., momentum equations are not solved for this solid phase). As in the experiment, the packing material is made of 1.6 cm polypropylene Pall rings with a specific surface area of 330 m^2/m^3. The critical surface tension needed by Eq. (15) is given a value of 61.25 dyns/cm [45]. As noted earlier, a uniform mean porosity is used in the simulation, which matches the experimentally reported value of $\epsilon = 0.93$.

The gas phase is defined as a mixture of air, CO_2 and H_2O vapor. The gas phase is considered slightly compressible using the ideal gas law. The gas phase viscosity is based on Sutherland's formula applied to air [46]. To fully close the chemical species mass balance equation (Eq. (3)) requires a value for the diffusion coefficient of the nth chemical species in its respective phase ($\mathcal{D}_{g,n}$ and $\mathcal{D}_{l,n}$). Here, a single diffusion coefficient is defined for each phase, as, $\mathcal{D}_{g,n} = D_g$ and $\mathcal{D}_{l,n} = D_l$. MFIX default models are taken for gas phase diffusivity, conductivity (λ_g) and specific heat (C_{pg}). In particular, the gas phase diffusivity is that of CO_2 in N_2 with the influence of gas temperature and pressure according to the Fuller relation [47]. The gas phase conductivity is set to that of air with a temperature dependency [48]. The specific heat of the gas phase is calculated based on mass average of the specific heat of each chemical species present.

For the MEA solvent, the liquid phase is defined as a mixture of H_2O, $CO_2(l)$, RNH_2, RNH_3^+, and $RNHCOO^-$. In the hydrodynamic model (Eqs. (1)-(4)), as opposed to the mass transfer model (described in Section 2.3.2), constant values of viscosity and density representative of 30 wt% MEA are used: i.e., 2.747 cP and 1.010 g/cm^3, respectively [2]. The liquid phase diffusivity is assigned a zero value, which is the

MFIX default. For the liquid phase conductivity the MFIX default model is used (see [42-43] for details), while the heat capacity of the liquid (C_{pl}) is based on that of MEA [49], i.e., $C_{pl} = 28.93 + 1.152x10^{-2}T + 9.567x10^{-5}T^2$ in units $\frac{cal}{mol \cdot K}$.

The boundary conditions are specified as follows: the liquid phase is introduced into the domain via a point source on the top of the column with a given mass flow rate uniformly distributed across the column. The liquid exits at the bottom of the column, where the gas phase enters the column through a pressure inlet boundary condition with a given pressure. Gas exits from the top of the column, which is modeled using a pressure outlet boundary condition with the outlet pressure specified as 0 gauge. The liquid at the inlet is either pure water or aqueous MEA of specified concentration; the gas at the inlet boundary is composed of 14% CO_2 and 86% air in molar fraction. The column sidewalls are modeled as no-slip boundaries with zero species fluxes for both gas and liquid species. The inlet and wall temperatures are set to 300 K for both gas and liquid, which represents the experimental operation. (The experiments were run in a cold flow scenario wherein the gas is introduced into the column at ambient conditions and allowed to react.)

The governing equations are discretized with a finite volume method and solved on a staggered grid. An iterative solution strategy based on SIMPLE [50] is employed, which couples the velocity and pressure. Spatial discretization of the convection term is achieved using a first-order accurate upwind scheme. A few simulations were repeated with a second-order accurate Superbee equation with deferred correction that qualitatively corroborates the behavior predicted in the former (results not shown). The predicted gas mass flow rate and overall liquid holdup are essentially identical to those predicted using the first-order upwind scheme. A variable time step procedure is used to optimize run time and convergence, where the time step is adjusted in small amounts over the course of the run. The minimum and maximum time steps are specified as 1E-8 and 1E-4, respectively. An averaged time-step of about 1E-5 is necessary. Numerical solution is obtained with a residual tolerance of less than 10^{-3} for all equations. For a complete list of the numerical parameters used in the simulation, see the MFIX user guide [43, 51]. The simulation was considered to reach

pseudo-steady state after 40 s (out of 60 s) without mass transfer and 80 s (out of 100 s) with mass transfer when the solvent mass outflow rate and the species concentrations at the outflow were approximately constant.

Three different numerical models for the cylindrical column were examined: 2D axial-symmetric cylindrical, 2D Cartesian, and 3D cylindrical. A convergence study for both hydrodynamics and mass transfer (details are presented in Section 3.2.4) indicated that the less expensive 2D cylindrical model with the resolution Δx = 1 cm was sufficiently accurate for this study and hence was employed in most simulations unless otherwise mentioned.

3.2 Results

After the counter-current flow reached a steady state, the simulation results were analyzed. In this section, the steady-state simulation predictions on hydrodynamics and CO_2 absorption are compared with those from experimental measurements [2] for calibration of model parameters and cross validation of the calibrated model. The parameters calibrated in the semi-empirical closure models include the equivalent particle diameter, nominal size of the packing structure and the wetting area model.

3.2.1 Pressure drop

In the experiment pressure drop versus varying gas inflow rate was measured while maintaining a constant liquid–gas ratio (*L/G*) for both water and 30 wt% MEA [2]. Here L and G refer to the volumetric flow rate of liquid and gas, respectively, which are related to superficial mass velocities (L' and G') presented earlier through the corresponding phase density and column cross-sectional area (A; e.g., $L = L'A/\rho_l$). Unlike the experiments where the gas velocity is specified as a controllable parameter resulting in the pressure that is measured, in the simulations the column pressure drop column is specified via the boundary conditions, while the inlet gas velocity (and mass flowrate) is predicted.

In the interphase interaction model, the particle diameter d_p in Eqs. (5) – (7) is defined as the equivalent particle diameter, which depends on the specific packing structure. Specifically, it depends on not only the shape and size of the packing elements but also the topology of how the elements are packed together. The packing used in the experiment corresponds to an equivalent particle diameter of 0.12 cm (computed as $d_p = 6\varepsilon_s/a$, which reflects the packing material in the column). Again, it is worth noting that the physical picture invoked to derive the interphase momentum transfer equations may not resemble that which is encountered in a solvent absorption, even when considering a random packing structure. The model of Attou et al. [23] employed in this work assumes that a packing surface is totally covered by a liquid film wherein the gas flows through a central zone of interstitial volume. However, the packing is often not completely wetted in solvent absorption, and hence quantifying the wetting area is an active area of research. Furthermore, in the model of Attou et al. [23], the packing was made of catalyst particles that are assumed spherical. However, in solvent absorption, the packing is made of structured-packing units or of individual elements of complex geometries designed to promote wetting and interfacial contact. And the resulting porosity is typically much higher (often greater than 90%) than those observed in literature of trickle bed reactors (around 60%).

In view of these differences, the equivalent particle diameter was not used in the simulations. Instead, the particle diameter was calibrated based on a single experimental operating condition so that the predicted gas flow rate at the specified pressure drop matches that observed experimentally. In the experiment [2], a pressure drop of 85 Pa/m was measured for the case of water at L/G=10.69 L/m^3 and $F - factor =$ 0.33 Pa$^{0.5}$. Note that the quantity $F - factor$ is related to the superficial gas velocity ($u_{gs} = \varepsilon_g|\boldsymbol{u}_g|$) and the square root of gas density as:

$$F - factor = u_{gs}\sqrt{\rho_g}. \tag{18}$$

Given $F - factor$, the superficial gas velocity can be calculated, and from that, the liquid flow rate can be determined based on the fixed value of L/G. In the simulation, the particle diameter was adjusted until the

predicted gas flow rate at the given pressure drop matched that of the experiment. This process yielded d_p= 0.15 cm, which is close to the equivalent particle diameter of the packing. The calibrated d_p was then used for predictions at other $F - factor$ values for both water and 30 wt% MEA, as shown in Fig. 1 and Fig. 2, respectively. Reasonable agreement between simulation results and experimental measurements was obtained with a maximum discrepancy of about 16%. Further agreement may be possible by including dispersion forces to reflect the liquid dispersion in the packing [52-54] or by using a more appropriate model for the interphase drag [15].

3.2.2 Liquid holdup

Values for liquid holdup were also reported for the air-water system at varying liquid flow rates (data for 30 wt% MEA were not available) while again keeping a constant *L/G* ratio. As the liquid loading increases more liquid is held in the packing leading to a smaller void fraction in the column. Here, the liquid holdup is taken as the average volume fraction of liquid in the packing portion of the column. This corresponds to total liquid holdup which is equal to the sum of a static and a dynamic holdup. It is not possible to extract a dynamic liquid holdup in the simulation. Therefore, to compare with the dynamic liquid holdup measured in the experiment, a formula for static holdup (ε_l^0) is used [20] to compute the dynamic holdup from the total liquid holdup predicted by the simulation:

$$\varepsilon_l^0 = \frac{1}{20+0.9E\ddot{o}}, \tag{19}$$

with the Eötvös number:

$$E\ddot{o} = \frac{\rho_l g d_p^2 (1-\varepsilon_s)^2}{\sigma \varepsilon_s^2}. \tag{20}$$

The notation here is as before. Fig. 3 shows how the total liquid holdup varies over time at the liquid loading of 0.326 $m^3/m^2/s$. After sufficient time (~35 s) the liquid holdup is observed to reach a steady state. Fig. 4 depicts the steady liquid holdup for water as a function of liquid loading. As expected, the dynamic liquid holdup increases with the increasing liquid loading. Furthermore, with the calibrated value of d_p

from the previous section, the predictions of simulations satisfactorily agree with the experimental measurements.

3.2.3 CO_2 absorption

The above comparisons for pressure drop and liquid holdup essentially correspond to cold-flow non-reactive conditions. Next, CO_2 absorption was examined for 30 wt% MEA with a lean loading of 0.0.03054 mole CO_2 per mole MEA. As in the experiment, the gas inlet CO_2 molar concentration was set at 14%. As CO_2 passed through the packed column and reacted with MEA, the concentration of CO_2 in the gas phase gradually decreased and eventually a steady state was reached. Snapshots of the mass fraction distributions for MEA, CO_2 in the gas phase, and RNH_3+ (reactive product) in the liquid phase are presented in Fig. 5 at two different times for $F - factor = 0.57\ \mathrm{Pa}^{0.5}$ and $L/G = 10.69\ \mathrm{L/m^3}$. Fig. 6 compares the liquid holdup, temperature and CO_2 along the column height after steady state has been reached for an $F - factor = 0.57\ \mathrm{Pa}^{0.5}$ at two different L/G ratios: $L/G = 10.69\ \mathrm{L/m^3}$ and $7.35\ \mathrm{L/m^3}$.

Once steady state was reached the concentration of CO_2 at the outlet was used to evaluate the CO_2 capture efficiency defined as:

$$\mathrm{CO_2\ capture\ efficiency} = \frac{X_{CO_2}^{inlet} - X_{CO_2}^{outlet}}{X_{CO_2}^{inlet}} \times 100\% . \tag{21}$$

Here, X_{CO_2} is the average mass fraction of CO_2 in gas phase across the column cross section.

The mass transfer closure model employed here (Eqs. (16) and (17)) was based on Onda's fitting to experimental data for packings of Raschig rings, Berl saddles, spheres, and rods [38]. As noted by Onda et al., this model lead to larger errors for some geometries and sizes, for instance, Raschig rings smaller than l.5 cm and Berl saddles smaller than 1/2". Recall the experiments from which we are comparing employed Pall rings having a nominal size (D_p) of 1.6 cm as the packing material. In view of this difference, the nominal particle size was calibrated for Pall rings. This was accomplished using a single experimental

operating condition so that the predicted CO_2 capture efficiency at the specified operating condition matched that observed in the experiment. Specifically, a CO_2 capture efficiency of 95% was measured at $F - factor = 0.57$ Pa$^{0.5}$ and $L/G = 10.69$ L/m^3, and D_p was adjusted until the predicted CO_2 capture efficiency matched. This process resulted in D_p= 3.0 cm, which is about twice the size of the Pall rings. The calibrated D_p was then used for predictions at other operating conditions consisting of two values of $F - factor$ and varying L/G ratios.

Fig. 7 presents the simulation results of CO_2 capture efficiency compared with the experimental data for 6 conditions (two values of $F - factor$ and three L/G ratios). As observed in the experiment, the computed CO_2 capture efficiency varies monotonically with liquid flow rate (or L/G ratio) for both values of $F - factor$. However, for L/G less than 6.68 L/m^3, the experimentally measured dependence of CO_2 capture efficiency on the L/G ratio was not properly captured by the simulations. Also, the difference of CO_2 capture efficiencies between the two different $F - factor$ was not reflected in the simulation results. These two discrepancies could result from the inaccurate estimation for the wetting area. Estimation of interfacial area is a topic of ongoing research. However, gas and liquid flow rates are likely to play a role [36]. Channeling and maldistribution may lead to incomplete wetting of the surface. Similarly, liquid surface area in dead zones may also result in lower effective interfacial area. Overprediction of the effective interfacial area by the current model may account for the discrepancies observed in Fig 7. Thus, the empirical wetting area model is adapted to the current system characterized by MEA through random packed Pall rings based on the experimental evidence for CO_2 capture efficiency.

Eq. (12) suggests that absorbed CO_2 flux (N_{CO_2}) is linearly dependent on the wetting area (a_w). Plotting N_{CO_2} versus a_w for eight experimental L/G ratios and a fixed value of $F - factor = 0.57$ Pa$^{0.5}$ (Fig. 8) confirms this observation over the selected operating conditions. In this figure, N_{CO_2} and a_w were effectively extracted from the corresponding MFIX simulations. Specifically, N_{CO_2} and a_w were evaluated

based on Eqs. (12) and (14)-(17) with E = 1 using simulation values for ε_g, ε_l, p_{CO_2}, and C_{CO_2}. It is worth noting that while k_l^o (Eq. (16)), and therefore $P_{CO_2}^{interface}$ (Eq. (14)), show some non-linear dependence on a_w, the resulting CO_2 flux is effectively linearly dependent on a_w for the conditions examined. This implies that, as expected, the wetting area model may be modified according to CO_2 capture efficiencies.

Recall, the aim here is simply to develop an improved CFD model that may be used to explore the impact of operating conditions of column performance, as opposed to developing a more fundamentally rigorous wetting area model. So, in this endeavor, a simple nonlinear fit is used for the two flow factors examined (e.g., Fig 7). Specifically, a second-order polynomial function of the form $f(v_l) = c_1 v_l^2 + c_2 v_l + c_3$ was fit based on minimizing the deviation between the simulation results $(\hat{y}_1, \hat{y}_2, \hat{y}_3)$ for CO_2 capture efficiency and the experimental data (y_1, y_2, y_3) at three L/G ratios (5.34, 8.02, 10.69 L/m^3 as noted in Fig. 7). Namely, the fit was made at each $F - factor$ such that (c_1, c_2, c_3) satisfies:

$$\min_{c_1,c_2,c_3} \sum_i [y_i - f(|\boldsymbol{u}_l|)\hat{y}_i]^2 \,. \tag{22}$$

In doing so the following fitted functions $f(v_l)$ are obtained:

$$f(v_l) = -9.05|\boldsymbol{u}_l|^2 + 9.53|\boldsymbol{u}_l| - 1.45 \quad \text{for } F - factor = 0.57 \text{ Pa}^{0.5} \,, \tag{23}$$

$$f(v_l) = -1.41|\boldsymbol{u}_l|^2 + 1.96|\boldsymbol{u}_l| + 0.17 \quad \text{for } F - factor = 0.69 \text{ Pa}^{0.5}. \tag{24}$$

So that the correlation for wetting area (a_w) may be expressed as:

$$\frac{a_w}{a_t} = f(|\boldsymbol{u}_l|)\left[1 - \exp\left(-1.45\frac{\sigma_c^{0.75} g^{0.05} L^{0.4}}{\sigma^{0.95} a_t^{0.35} \mu_l^{0.1} \rho_l^{0.1}}\right)\right]. \tag{25}$$

Here, the original formulation by Onda et al. [38] is augmented by a multiplier function $f(|\boldsymbol{u}_l|)$ that depends on the gas velocity. To show how the new correlation influences the predicted wetting area, it is plotted and compared to the original formulation in Fig. 9. Notably, the new correlation displays a much stronger dependence of wetting on gas and liquid flow rates.

The improved correlation for wetting area was then used for prediction of CO_2 capture efficiency over all experimental conditions (i.e., for the two gas velocities and all L/G ratios) as presented in Fig. 10. Overall, the simulation results agree with the experimental data for all gas and liquid flow rates.

3.2.4 Effects of numerical setup and mesh size

Convergence of simulation results for both hydrodynamics and mass transfer was also examined in terms of the predicted gas velocities and CO_2 capture efficiencies. Different simulation setups and numerical resolutions were tested under the same operating conditions. As summarized in Table 1, three different numerical models at two different resolutions produced converged results. Thus, most simulations employed the less expensive 2D cylindrical model with the coarser resolution, Δx = 1 cm.

4. Discussion

We have presented device-scale CFD simulations of CO_2 capture in an amine-based absorber column with randomly packed Pall rings. The simulations were based on a multi-phase Eulerian porous-media model with empirical closures for hydrodynamics and mass transfer. Since the physical picture and features of packing structures invoked to derive the literature-reported empirical closure models may not resemble what occurred in the solvent absorption studied herein, the parameters in the empirical models were calibrated using the available experimental data. For that, we proposed a hierarchical calibration approach to make the empirical closure models applicable for our specific absorber and operating conditions. Namely, the parameter in the hydrodynamic model was first calibrated to correctly capture the hydrodynamics. With the calibrated hydrodynamic parameter, the parameters in the model of mass transfer were in turn calibrated to match the experimental CO_2 capture efficiency. For each calibration, cross validations were performed using the held-out experimental data under different operating conditions other than those used for calibrations.

First, the effective particle diameter d_p in the interphase drags for the momentum transfer between phases was calibrated based on a single experimental operating condition so that the predicted gas flow rate at the specified pressure drop matches that observed experimentally. It yielded d_p = 0.15 cm, close to the equivalent particle diameter of Pall rings used in this work. With it, we computed gas flow rates at other pressure drops for both water and 30% MEA and dynamic liquid holdups at different liquid flow rates for water. Good agreement was obtained between the simulation results and experimental data using this single parameter calibrated for hydrodynamics. Next, the nominal size of the packing material, D_p, in the mass transfer model was calibrated so that the predicted CO_2 capture efficiency at a specific operating condition matched that of the experiment. A value of D_p= 3.0 cm was determined, which is comparable to the nominal size of the Pall rings used here. Given that the wetting area may be poorly characterized at varied gas and liquid flow rates, the empirical model for wetting area was further calibrated. Specifically, a modified model for wetting area was developed for two flow factor values using three L/G ratios each. As a result, the dependence of the wetting area model on the gas and liquid flow rates increased especially at lower values of L/G. With the above hierarchical calibration approach, the predicted CO_2 capture efficiencies at different $L/$□ ratios for each gas velocity are in satisfactory agreement with the experimental measurements in the present randomly packed Pall Ring. The same hierarchical approach can be applied to develop device-scale CFD models of solvent absorption for other packings (structured or random).

It is worth mentioning that device-scale CFD models have the potential to capture flow heterogeneities in the form of poor wetting, channeling and bypassing in the packing bed. These are all potential issues limiting the device-scale capture performance which cannot be captured by a 1D process model. However, this is beyond the scope of the present work.

Finally, it is possible that a high fidelity multi-scale CFD model be developed in the future. In the literature, Raynal and Royon-Lebeaud presented a multiscale CFD simulation approach that couples CFD predictions from the corrugation scale, the periodic element scale of the real structured-packing, and the column scale [55]. In that, the liquid holdup was computed on the corrugation surface by a gas-liquid 2D model; the pressure

drop was obtained at the element scale by a gas phase 3D model; and the gas-liquid distributions was then studied at the column scale by a porous-media device-scale model. An alternative approach is currently being explored which employs VOF-based CFD simulations at the corrugation and element scales to develop the hydrodynamic and mass transfer closure models [56-58]. These closure models can then be applied in the porous-media device-scale CFD model for predictions of pressure drop, liquid holdup, and CO_2 absorption of the entire device.

Acknowledgments

W.P. acknowledges partial support from Pacific Northwest National Laboratory (PNNL). This work was also supported by the U.S. Department of Energy's (DOE) Office of Fossil Energy's Carbon Capture Simulation Initiative (CCSI) through the National Energy Technology Laboratory. Pacific Northwest National Laboratory is operated by Battelle for DOE under Contract DE-AC05-76RL01830.

Notations

a	interfacial surface area per unit volume of bed
a_t	total surface area of packing per unit volume of bed
a_w	wetting surface area of packing per unit volume of bed
C_{CO_2}	molar concentration of CO_2 in the bulk
$C_{CO_2}^{interface}$	molar concentration of CO_2 in the interface
C_{pi}	i^{th} phase mixture specific heat
d_p	surface-volume equivalent sphere diameter of the particles
$\mathcal{D}_{in}$	n^{th} species diffusion coefficient of the nth species in the ith phase
$\mathcal{D}_{g,s}$	diffusivity of the solute species in the gas phase
$\mathcal{D}_{l,s}$	diffusivity of the solute in the liquid phase

D_p	nominal size of the packing material
E	enhancement factor
$\mathbf{g}$	gravitational acceleration
G'	superficial mass velocity of the gas
H	Henry's solubility constant
k_2	2nd order reaction rate constant
k_g	physical mass transfer coefficients of the CO_2 species in the gas phase
k_l^{o}	physical mass transfer coefficients of the CO_2 species in the liquid phase
L'	superficial mass velocity of the liquid
N_i	number of chemical species comprising the ith phase
p_{CO_2}	partial pressure of CO_2 in the bulk
$p_{CO_2}^{\mathrm{interface}}$	partial pressure of CO_2 in the interface
P_i	th phase pressure
R	universal gas constant
R_{in}	rate of formation of the nth species in the ith phase
S_p	area of the particle
T_i	i^{th} phase temperature
$\mathbf{u_i}$	cell velocity of the ith phase
V_p	volume of the particle
X_{in}	n^{th} species mass fraction of the nth species in the ith phase

Dimensionless Number

$Eö$	Eötvös number

Greek letters

μ_i	viscosity of the ith phase
ε_l^0	static holdup
σ	surface tension of liquid
σ_c	critical surface tension of packing material
ε_i	volume fraction of the ith phase
ρ_i	density fraction of the ith phase
$\boldsymbol{\tau}_i$	shear stress
λ_i	i^{th} phase thermal conductivity

Reference

1. Grosser, K.; Carbonell, R. G.; Sundaresan, S., Onset of Pulsing in Two-Phase Cocurrent Downflow through a Packed Bed. *AIChE Journal* **1985,** *34* (11), 1850-1860.
2. Chen, Z. S.; Yates, D.; Neathery, J. K.; Liu, K. L., The effect of fly ash on fluid dynamics of CO2 scrubber in coal-fired power plant. *Chem Eng Res Des* **2012,** *90* (3A), 328-335.
3. Notz, R.; Mangalapally, H. P.; Hasse, H., Post combustion CO2 capture by reactive absorption: Pilot plant description and results of systematic studies with MEA. *International Journal of Greenhouse Gas Control* **2012,** *6*, 84-112.
4. Tsai, R. E.; Seibert, A. F.; Eldridge, R. B.; Rochelle, G. T., A Dimensionless Model for Predicting the Mass-Transfer Area of Structured Packing. *Aiche Journal* **2011,** *57* (5), 1173-1184.
5. Mackowiak, J., *Fluid Dynamics of Packed Columns*. Springer-Verlag Berlin Heidelberg: 2010.
6. Raynal, L.; Ben Rayana, F.; Royon-Lebeaud, A., Use of CFD for CO2 absorbers optimum design : from local scale to large industrial scale. *Energy Procedia* **2009,** *1* (1), 917-924.
7. Raynal, L.; Boyer, C.; Ballaguet, J. P., Liquid holdup and pressure drop determination in structured packing with CFD simulations. *Can J Chem Eng* **2004,** *82* (5), 9.
8. Owens, S. A.; Perkins, M. R.; Eldridge, R. B.; Schulz, K. W.; Ketcham, R. A., Computational Fluid Dynamics Simulation of Structured Packing. *Industrial & Engineering Chemistry Research* **2013,** *52* (5), 2032-2045.
9. Tung, V. X.; Dhir, V. K., A Hydrodynamic Model for 2-Phase Flow through Porous-Media. *Int J Multiphas Flow* **1988,** *14* (1), 47-65.
10. Asendrych, D.; Niegodajew, P.; Drobniak, S., Cfd Modelling of Co2 Capture in a Packed Bed by Chemical Absorption. *Chem Process Eng-Inz* **2013,** *34* (2), 269-282.

11. Fourati, M.; Roig, V.; Raynal, L., Liquid dispersion in packed columns: Experiments and numerical modeling. *Chemical Engineering Science* **2013,** *100*, 266-278.
12. Iliuta, I.; Petre, C. F.; Larachi, F., Hydrodynamic continuum model for two-phase flow structured-packing-containing columns. *Chemical Engineering Science* **2004,** *59* (4), 879-888.
13. Pham, D. A.; Lim, Y. I.; Jee, H.; Ahn, E.; Jung, Y., Porous media Eulerian computational fluid dynamics (CFD) model of amine absorber with structured-packing for CO2 removal. *Chemical Engineering Science* **2015,** *132*, 259-270.
14. Kim, J.; Pham, D. A.; Lim, Y. I., Gas-liquid multiphase computational fluid dynamics (CFD) of amine absorption column with structured-packing for CO2 capture. *Comput Chem Eng* **2016,** *88*, 39-49.
15. Finn, J. R.; Galvin, J. E., Calibration of drag models for mesoscale simulation of gas-liquid flow through packed beds. *Chemical Engineering Science* **2017,** *172*, 722-730.
16. Jiang, Y.; Khadilkar, M. R.; Al-Dahhan, M. H.; Dudukovic, M. P., CFD of multiphase flow in packed-bed reactors: I. k-fluid modeling issues. *Aiche Journal* **2002,** *48* (4), 701-715.
17. Dudukovic, M. P.; Larachi, F.; Mills, P. L., Multiphase catalytic reactors: a perspective on current knowledge and future trends. *Catalysis Reviews: Science and Engineering* **2002,** *44* (1), 123-246.
18. Gunjal, P. R.; Kashid, M. N.; Ranade, V. V.; Chaudhari, R. V., Hydrodynamics of trickle-bed reactors: Experiments and CFD modeling. *Industrial & Engineering Chemistry Research* **2005,** *44* (16), 6278-6294.
19. Musser, J.; Syamlal, M.; Shahnam, M.; Huckaby, D., Constitutive equation for heat transfer caused by mass transfer. *Chem Eng Sci* **2015,** *123*, 436-443.
20. Saez, A. E.; Carbonell, R. G., Hydrodynamic Parameters for Gas-Liquid Cocurrent Flow in Packed-Beds. *AIChE Journal* **1985,** *31* (1), 52-62.
21. Holub, R. A.; Dudukovic, M. P.; Ramachandran, P. A., A Phenomenological Model for Pressure-Drop, Liquid Holdup, and Flow Regime Transition in Gas-Liquid Trickle Flow. *Chemical Engineering Science* **1992,** *47* (9-11), 2343-2348.
22. Iliuta, I.; Larachi, F., The generalized slit model: pressure gradient, liquid holdup & wetting efficiency in gas-liquid trickle flow. *Chemical Engineering Science* **1999,** *54*, 5039-5045.
23. Attou, A.; Boyer, C.; Ferschneider, G., Modelling of the hydrodynamics of the cocurrent gas-liquid trickle flow through a trickle-bed reactor. *Chemical Engineering Science* **1999,** *54* (6), 785-802.
24. Gunjal, P. R.; Ranade, V. V., Modeling of laboratory and commercial scale hydro-processing reactors using CFD. *Chemical Engineering Science* **2007,** *62* (18-20), 5512-5526.
25. Kuzeljevic, Z. V.; Dudukovic, M. P., Computational Modeling of Trickle Bed Reactors. *Industrial & Engineering Chemistry Research* **2012,** *51* (4), 1663-1671.
26. Jiang, Y.; Khadilkar, M. R.; Al-Dahhan, M. H.; Dudukovic, M. P., CFD of multiphase flow in packed-bed reactors: II. Results and applications. *Aiche Journal* **2002,** *48* (4), 716-730.
27. Aboudheir, A.; Tontiwachwuthikul, P.; Chakma, A.; Idem, R., Kinetics of the reactive absorption of carbon dioxide in high CO2-loaded, concentrated aqueous monoethanolamine solutions. *Chemical Engineering Science* **2003,** *58* (23-24), 5195-5210.
28. Khan, F. M.; Krishnamoorthi, V.; Mahmud, T., Modelling reactive absorption of CO_2 in packed columns for post-combustion carbon capture applications. *Chem Eng Res Des* **2011,** *89* (9A), 1600-1608.
29. Tontiwachwuthikul, P. New pilot plant technique for designing gas absorbers with chemical reactions. Ph.D., University of British Columbia, 1991.
30. Astarita, G., *Mass transfer with chemical reactions*. Elseveir Publishing Company: Amsterdam/London/New York, 1967.
31. Hikita, H.; Asai, S.; Ishikawa, H.; Honda, M., The kinetics of reactions of carbon dioxide with monoethanolamine, diethanolamine and triethanolamine by a rapid mixing method. *The Chemical Engineering Journal* **1977,** *13*, 7-12.

32. Levenspiel, O., *Chemical Reaction Engineering*. 3rd ed.; John Wiley & Sons, Inc.: New York, USA, 1999.
33. Pandya, J. D., Adiabatic Gas-Absorption and Stripping with Chemical-Reaction in Packed Towers. *Chemical Engineering Communications* **1983,** *19* (4-6), 343-361.
34. Hiwale, R.; Hwang, S.; Smith, R., Model Building Methodology for Multiphase Reaction Systems-Modeling of CO2 Absorption in Monoethanolamine for Laminar Jet Absorbers and Packing Beds. *Industrial & Engineering Chemistry Research* **2012,** *51* (11), 4328-4346.
35. Versteeg, G. F.; Vanswaaij, W. P. M., Solubility and Diffusivity of Acid Gases (Co2, N2o) in Aqueous Alkanolamine Solutions. *J Chem Eng Data* **1988,** *33* (1), 29-34.
36. Wang, G. Q.; Yuan, X. G.; Yu, K. T., Review of mass-transfer correlations for packed columns. *Industrial & Engineering Chemistry Research* **2005,** *44* (23), 8715-8729.
37. Razi, N.; Bolland, O.; Svendsen, H., Review of design correlations for CO2 absorption into MEA using structured packings. *International Journal of Greenhouse Gas Control* **2012,** *9*, 193-219.
38. Onda, K.; Takeuchi, H.; Okumoto, Y., Mass transfer coefficients between gas and liquid phases in packed columns. *Journal of Chemical Engineering of Japan* **1968,** *1* (1), 56-62.
39. Versteeg, G. F.; van Swaaij, W. P. M., Solubility and Diffusivity of Acid Gases (CO2, N2O) in Aqueous Alkanoalmine Solutions. *J Chem Eng Data* **1988,** *33*, 29-34.
40. Weiland, R. H.; Dingman, J. C.; Cronin, D. B.; Browning, G. J., Density and viscosity of some partially carbonated aqueous alkanolamine solutions and their blends. *J Chem Eng Data* **1998,** *43* (3), 378-382.
41. Vazquez, G.; Alvarez, E.; Navaza, J. M.; Rendo, R.; Romero, E., Surface tension of binary mixtures of water plus monoethanolamine and water plus 2-amino-2-methyl-1-propanol and tertiary mixtures of these amines with water from 25 degrees C to 50 degrees C. *J Chem Eng Data* **1997,** *42* (1), 57-59.
42. Syamlal, M., W.A. Rogers, and T. O'Brien, MFIX documentation and theory guid. *DOE/METC94/1004, NTIS DE94000087.* **1993,** *U.S. Department of Energy, Office of Fossil Energy*, 1-57.
43. NETL, MFS NETL Multiphase Flow Science: Home of the MFIX Software Suite. https://mfix.netl.doe.gov/ **2015**.
44. Gabrielsen, J.; Michelsen, M. L.; Stenby, E. H.; Kontogeorgis, G. M., A Model for Estimating CO2 Solubility in Aqueous Alkanolamines. *Industrial & Engineering Chemistry Research* **2005,** *44* (9), 3348-3354.
45. Pacheco, M. A. Mass Transfer, Kinetics and Rate-based Modeling of Reactive Absorption. Ph.D., University of Texas, Austin, Texas, 1998.
46. Sutherland, W., The viscosity of gases and molecular force. *Philosophical Magazine Series 5* **1893,** *36* (223), 507-531.
47. Fuller, E. N.; Schettler, P. D.; Giddings, J. C., A new method for prediction of binary gas-phase diffusion coefficients. *Industrial and Engineering Chemistry* **1966,** *58* (5), 18-27.
48. Bird, B. R.; Stewart, W. E.; Lightfoot, E. N., Transport Phenomena. *New York: John Wiley & Sons* **1960**.
49. Dugas, R.; Alix, P.; Lemaire, E.; Broutin, P.; Rochelle, G., Absorber model for CO_2 capture by monoethanolamine - application to CASTOR pilot results. *Energy Procedia* **2009,** *1*, 103-107.
50. Patankar, S. V., Numerical Heat Transfer and Fluid Flow. *Taylor & Francis* **1980**.
51. NETL, Mfix User Guide 2015-1. https://mfix.netl.doe.gov/mfix/mfix-documentation/ **2015**.
52. Lappalainen, K.; Manninen, M.; Alopaeus, V., CFD modeling of radial spreading of flow in trickle-bed reactors due to mechanical and capillary dispersion. *Chemical Engineering Science* **2009,** *64* (2), 207-218.
53. Lappalainen, K.; Gorshkova, E.; Manninen, M.; Alopaeus, V., Characteristics of liquid and tracer dispersion in trickle-bed reactors: Effect on CFD modeling and experimental analyses. *Comput Chem Eng* **2011,** *35* (1), 41-49.

54. Solomenko, Z.; Haroun, Y.; Fourati, M.; Larachi, F.; Boyer, C.; Augier, F., Liquid spreading in trickle-bed reactors: Experiments and numerical simulations using Eulerian-Eulerian two-fluid approach. *Chemical Engineering Science* **2015,** *126*, 698-710.
55. Luo, X.; Hartono, A.; Hussain, S.; Svendsen, H. F., Mass transfer and kinetics of carbon dioxide absorption into loaded aqueous monoethanolamine solutions. *Chemical Engineering Science* **2015,** *123*, 57-69.
56. Wang, C.; Xu, Z.; Lai, C.; Whyatt, G.; Marcy, P.; Sun, X., Hierarchical calibration and validation for modeling bench-scale solvent-based carbon capture. Part 1: Non-reactive physical mass transfer across the wetted wall column. *Greenhouse Gases: Science and Technology* **2017**.
57. Singh, R. K.; Galvin, J. E.; Sun, X., Three-dimensional simulation of rivulet and film flows over an inclined plate: Effects of solvent properties and contact angle. *Chemical Engineering Science* **2016,** *142*, 244-257.
58. Singh, R. K.; Galvin, J. E.; Whyatt, G. A.; Sun, X., Breakup of a liquid rivulet falling over an inclined plate: Identification of a critical Weber number. *Physics of Fluids* **2017,** *29* (05), 052101.

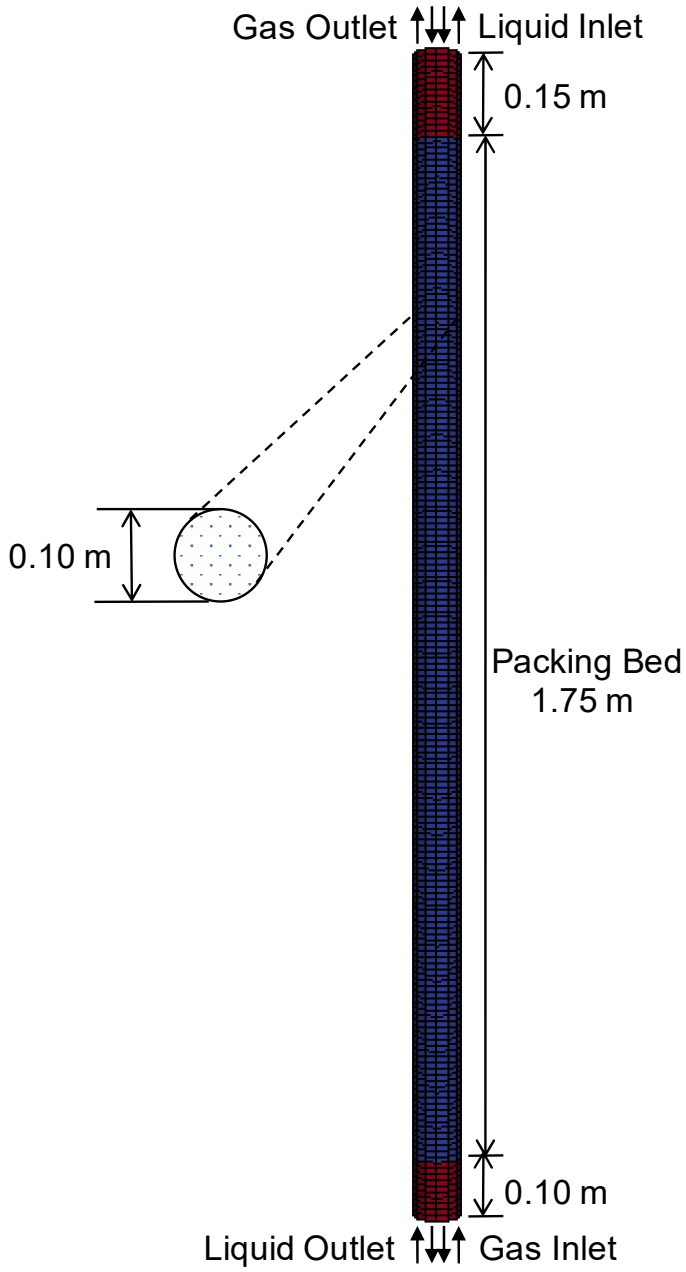

Figure 1. Geometry and mesh of CFD simulation domain for an amine absorber.

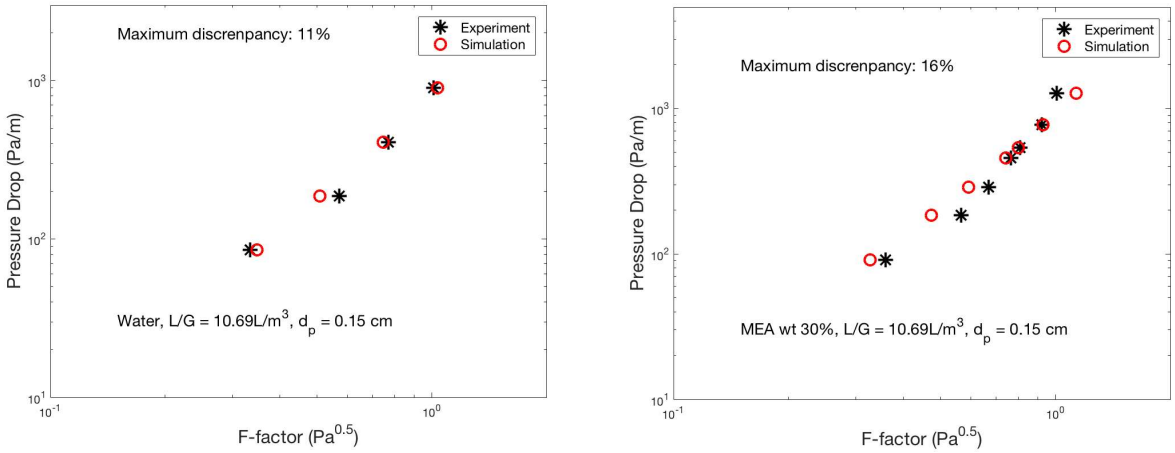

(a) Water (b) 30 wt% MEA

Figure 2. Pressure drop vs. F-factor predicted from MFIX simulations and compared with experimental data [2] for two different liquids.

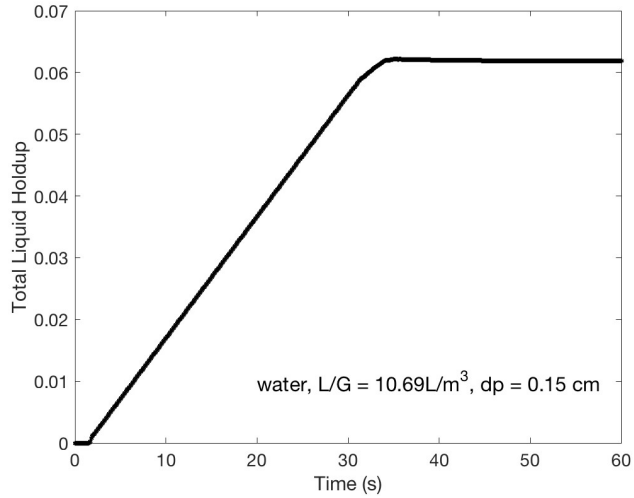

Figure 3. Total liquid holdup predicted from MFIX simulations with time for water and a liquid loading of 0.326 $m^3/m^2/s$.

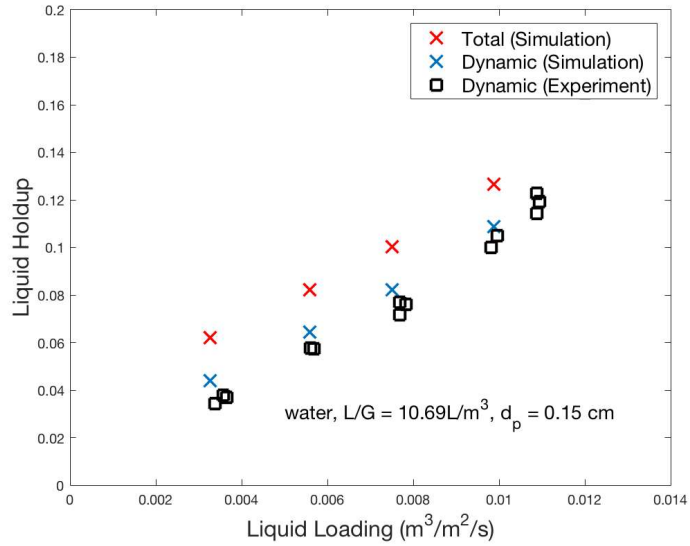

Figure 4. Liquid holdup of water predicted from MFIX simulations, compared with the experimental data [2].

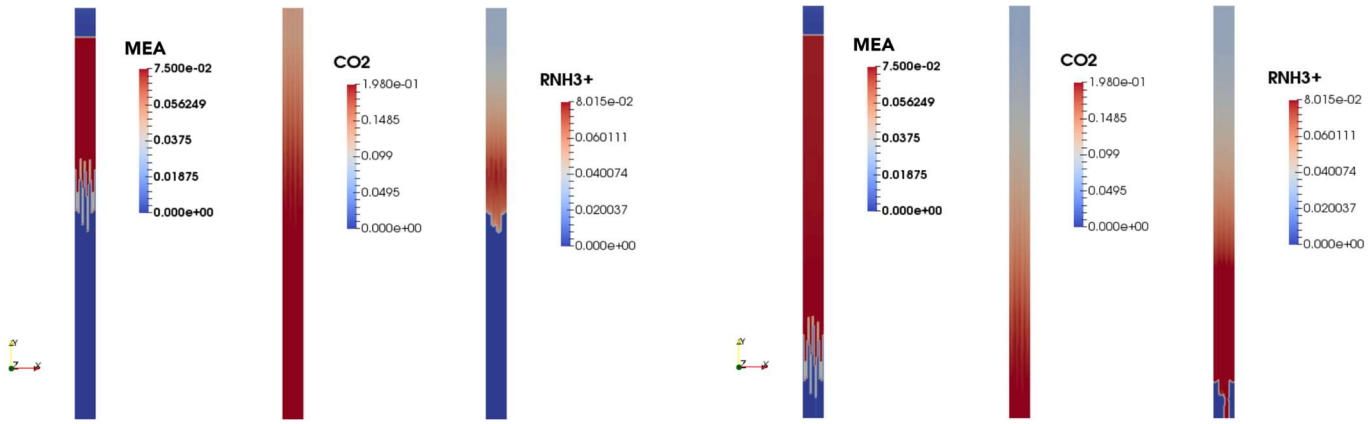

(a) Snapshot at $t = 20s$ (b) Snapshot at $t = 40s$

Figure 5. Contours of species mass fractions for MEA, CO_2, and reactive product RNH_3+ in a 2D Cartesian column.

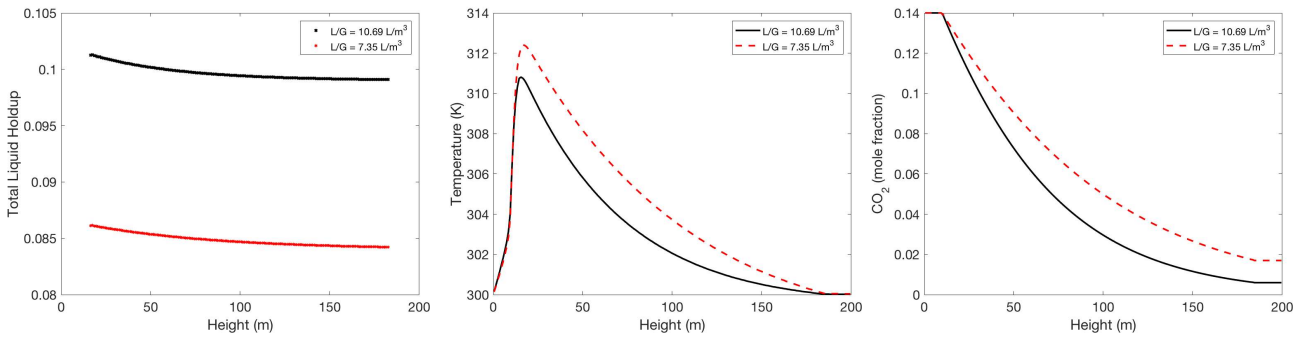

(a) (b) (c)

Figure 6. The area-averaged (a) liquid holdup (in the packing section), (b) temperature and (c) CO_2 with respect to the column height after the steady state for $F - factor = 0.57\ \mathrm{Pa}^{0.5}$.

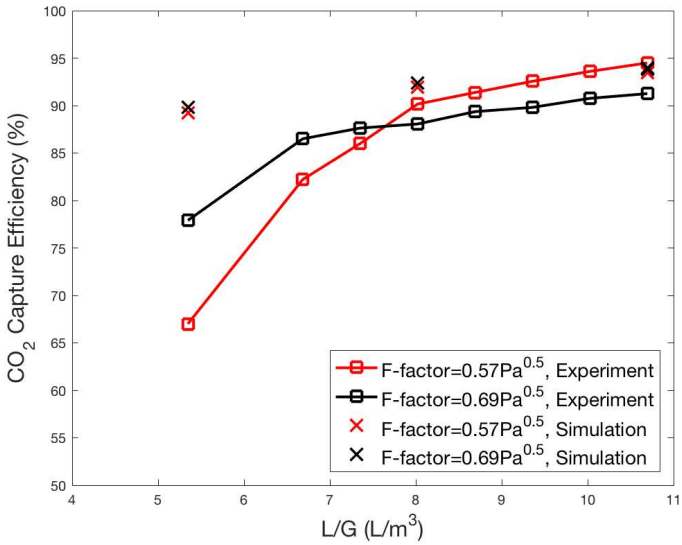

Figure 7. CO_2 capture efficiency vs. L/G ratio for 30 wt% MEA at two gas velocities computed from MFIX simulations, compared with the experimental measurements.

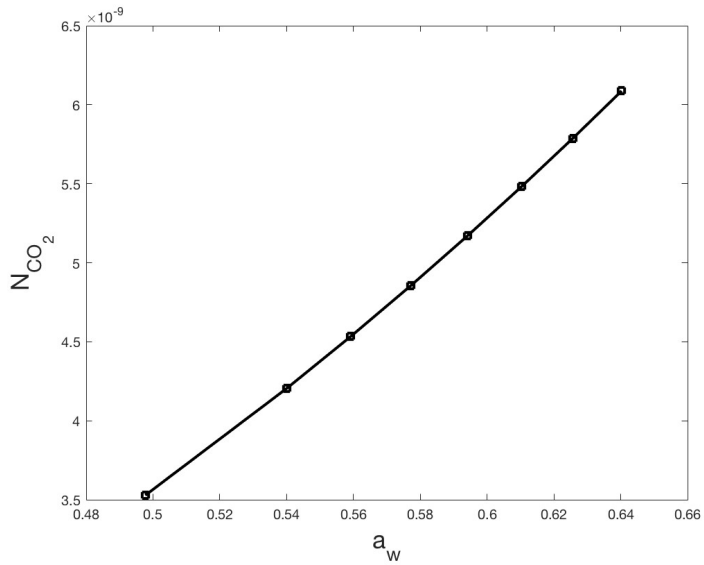

Figure 8. The absorbed CO_2 flux (N_{CO_2}) vs. wetting area (a_w).

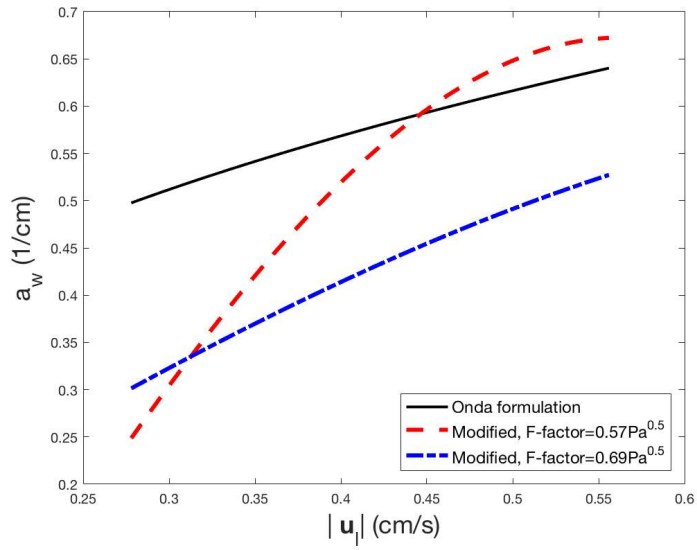

Figure 9. Wetting area (a_w) vs. liquid inflow velocity $|\boldsymbol{u}_l|$ predicted by the original Onda's and modified formulations.

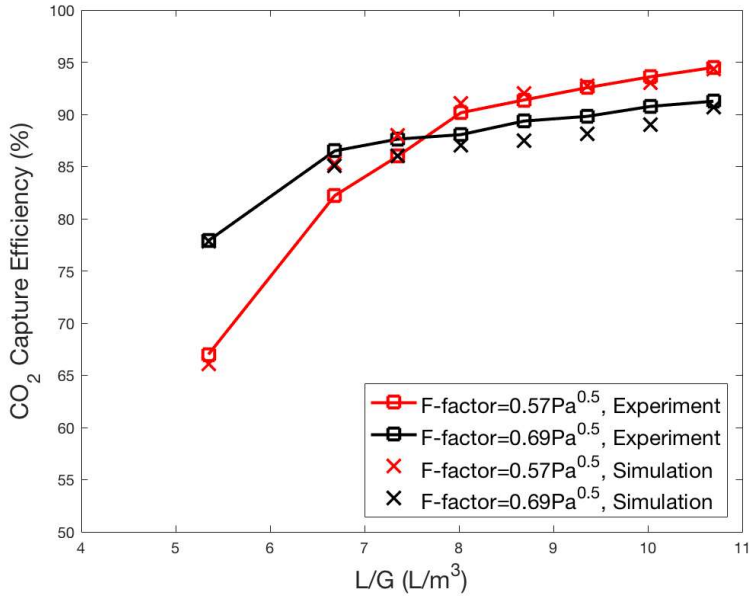

Figure 10. CO_2 capture efficiency vs. L/G ratio for 30 wt% MEA at two gas velocities computed from MFIX simulations using the modified correlation of wetting area, compared with the experimental measurements.

Table 1. Gas velocity and CO_2 capture efficiency predicted under the same operating condition using different simulation setups and numerical resolutions.

Simulation Setup		v_g (m/s)	CO_2 Capture Efficiency (%)
2D Cylindrical	Δx = 1 cm	0.5167	69.73
	Δx = 0.5 cm	0.5161	69.72
2D Cartesian	Δx = 1 cm	0.5166	69.73
	Δx = 0.5 cm	0.5195	70.24
3D Cylindrical	Δx = 1 cm	0.5166	69.73